R2-D.2: Optimization of Explosives Sensor Placement in Airports

I. PARTICIPANTS

Faculty/Staff			
Name	**Title**	**Institution**	**Email**
Qingyan "Yan" Chen	PI	Purdue University	yanchen@purdue.edu
Graduate, Undergraduate and REU Students			
Name	**Degree Pursued**	**Institution**	**Month/Year of Graduation**
Wei Liu	PhD	Purdue University	12/2017

II. PROJECT DESCRIPTION

Core funding for this project ends in Year 3 per the outcome of the Biennial Review process. Wei Lu, the PhD student working on this project, will be supported via ALERT core funds so as to not impact his degree completion. Results of the student work will be reported in a special section of the ALERT Year 4 Annual Report.

A. Project Overview

Effective detection of explosives-related threats is very important to the country and the world. In the past, the explosives detection community has invested heavily in contact sensing for portal screening. However, they are unable to answer the question: "Great sensors, but how do you know the vapors/particles get there?" This is because an airport is a large space, so the concentration of the vapors/particles of explosives are generally low. It is difficult to direct the low concentration of explosives agents to the limited amount of sensors. Therefore, our ALERT Phase 2 Year 2 project investigated how explosives vapors/particles were transported at the Indianapolis International Airport terminal; identified strategies that can be used to increase explosive vapor concentrations; and demonstrated how to use these strategies to detect explosives with suitable sensors. Computational fluid dynamics (CFD) simulations were used for predictions of air distribution and contaminant transport because they are more accurate than other numerical tools, and much faster than experimental measurements. Since this application is for airports, the space is much larger than those in the previous studies. Thus, CFD was found to be very expensive when it is used to find optimal sensor locations and to identify source positions. Therefore, our ALERT Phase 2 Year 3 project developed and validated the fast fluid dynamics (FFD), which was a faster method than CFD while maintaining the accuracy. The research can provide effective methods to detect explosives vapors in airports.

B. Biennial Review Results and Related Actions to Address

This project was slated for sunset in the last Biennial Review and was concluded at the end of Year 3. Through discussion following the Biennial Review process, the ALERT Director allocated ALERT core funding to be used in Year 4 to support Wei Lu, a Ph.D. candidate working on this project.

The major strength of this project is that the developed FFD solvers can be almost 40 times faster than CFD in predicting transient flow. The major weakness is that the developed FFD solvers do not have the user interface. It requires a lot coding to use it, which limits its application in the engineering field. Therefore, our

Year 4 project plans to develop the user interface for the FFD solvers. The work will be done by Mr. Liu as part of his Ph.D. requirement.

C. State of the Art and Technical Approach

Optimal sensor placement in an enclosed space requires predictions on air distribution and contaminant transport. As summarized by Chen [1], the numerical tools include nodal models (multi-zone model and zonal model) and CFD simulation. The nodal models can be very fast, but they only provide averaged characteristics of airflows and contaminant distributions within particular zones [2]. Significant errors may arise in large indoor spaces with stratified ventilation systems or strong jet momentums [3, 4]. Thus, the accuracy of a nodal model depends on the user's ability to identify different flow characteristics in different regions. CFD simulation provides the most detailed information about distributions of air velocity, temperature, contaminant dispersion, etc. When it is used for indoor airflow simulations, CFD is also the most accurate approach, as it involves the fewest assumptions. CFD simulation is therefore the most popular method used today in practice [1]. However, this method requires a powerful computer in order to handle a large number of grids for a large or complex indoor space, and the computing time can be very long [5]. A faster method is desired that can provide the same detailed indoor airflow information as CFD, and the same efficiency as the nodal models.

FFD, which solves the Navier-Stokes equations with a projection method, seems to meet the above requirements. FFD has been widely applied to weather prediction and the study of atmospheric flows [6, 7, 8, 9]. Since the major development by Stam [10] in the area of computer games, FFD has been used for flow simulations. Zuo and Chen [11] applied FFD to fast two-dimensional (2D) airflow simulations in an indoor environment and found that FFD can offer much more detailed flow information than do nodal models, with faster-than-real-time simulation speeds. Zuo et al. [12, 13] further improved the accuracy of FFD simulations by using the finite volume method, mass conservation correction, and a hybrid interpolation scheme. Recently, Jin et al. [14, 15, 16] extended FFD to the solution of three-dimensional (3D) airflow and proposed a conservative SL scheme to ensure the conservation of energy and species concentration. Those efforts have made FFD simulations of indoor airflow a viable alternative to CFD simulations, achieving similar accuracy with low computing time and computational capacity.

Nevertheless, there are some limitations associated with using FFD for indoor airflow simulations. The FFD solver developed by Zuo et al. [11] and Jin et al. [14] is applicable only to a hexahedral mesh, which cannot provide a sufficiently accurate depiction of a complex geometry such as the occupants of an indoor space. Besides, the current FFD solvers applied a semi-Lagrangian scheme to solve the advection term that would bring in significant numerical diffusion. The advantage is that the numerical diffusion could be used as the substitution of turbulent diffusion, so no extra turbulence model is needed. However, the significance of the numerical diffusion is determined by the mesh size and time step size. These two parameters are hard to determine so that the correct predictions could be obtained. Therefore, it is essential to develop FFD further for unstructured meshes that can be used to describe complex geometry and add turbulence models to FFD models without a semi-Lagrangian scheme to make it more stable and accurate. This report shows our effort in implementing FFD models in OpenFOAM (Open Field Operation and Manipulation) [17], an open-source CFD program with the capacity to handle a variety of unstructured meshes. To ensure the validity and accuracy of our implementation, this report also describes the validation of FFD simulation for predicting different indoor airflow with experimental air distribution data from the literature.

D. Major Contributions

This section discusses the fundamentals of FFD and provides the corresponding validations.

D.1. Fast fluid dynamics

FFD solves the Navier-Stokes equations in a similar manner to CFD. For incompressible viscous flow in an indoor environment, the Navier-Stokes equations are:

$$\frac{\partial U_i}{\partial x_i} = 0 \tag{1}$$

$$\frac{\partial U_i}{\partial t} + U_j \frac{\partial U_i}{\partial x_j} = -\frac{1}{\rho}\frac{\partial p}{\partial x_i} + \nu \frac{\partial^2 U_i}{\partial x_j \partial x_j} + \frac{1}{\rho} F_i \tag{2}$$

where i, j = 1, 2, and 3. The variable U_i is the i^{th} component of the velocity vector, p is pressure, ρ is density, F_i is the i^{th} component of the body forces, and v is kinetic viscosity. The previous studies used the non-incremental pressure-correction scheme with semi-Lagrangian (NIPC-SL) scheme to solve the above Navier-Stokes equations. This project implemented this scheme and another three pressure-correction schemes: non-incremental pressure-correction (NIPC) scheme, standard incremental pressure-correction (SIPC) scheme, and rotational incremental pressure-correction (RIPC) scheme in OpenFOAM.

Non-incremental pressure-correction scheme

The NIPC scheme is the simplest pressure-correction scheme that was originally proposed by Chorin [18] and Temam [19]. It applies a two-step time-advancement scheme that splits the momentum equation (Eq. (2)) into two discretized equations:

$$\frac{U_i^* - U_i^n}{\Delta t} = -U_j^n \frac{\partial U_i^*}{\partial x_j} + \nu \frac{\partial^2 U_i^*}{\partial x_j \partial x_j} + \frac{1}{\rho} F_i \tag{3}$$

$$\frac{U_i^{n+1} - U_i^*}{\Delta t} = -\frac{1}{\rho}\frac{\partial p}{\partial x_i} \tag{4}$$

where U^n and U^{n+1} represent the velocity at the previous and current time step, respectively. U^* is intermediate velocities. To resolve the coupled pressure and velocity, the method uses the pressure projection [20], which substitutes Eq. (4) into Eq. (1) to produce:

$$\frac{\partial^2 p}{\partial x_i \partial x_i} = \frac{\rho}{\Delta t}\frac{\partial U_i^*}{\partial x_i} \tag{5}$$

The NIPC scheme first solves Eq. (3) with the implicit Euler scheme for the temporal term; semi-implicit scheme for convection term; and implicit scheme for the diffusion term to obtain intermediate velocity U^*. Then the NIPC scheme solves the Poisson equation, Eq. (5), to obtain the pressure p. Finally, the NIPC scheme calculates the velocity at the next step U^{n+1} by solving Eq. (4). In OpenFOAM, the solution of Eqs. (3) and (5) is straightforward.

Standard incremental pressure-correction scheme

As observed by Goda [21], the pressure term is missing in Eq. (3) and adding the pressure gradient of the previous step would increase the accuracy. Then the two discretized equations are:

$$\frac{U_i^* - U_i^n}{\Delta t} = -\frac{1}{\rho}\frac{\partial p^n}{\partial x_i} - U_j^n \frac{\partial U_i^*}{\partial x_j} + \nu \frac{\partial^2 U_i^*}{\partial x_j \partial x_j} + \frac{1}{\rho} F_i \tag{6}$$

$$\frac{U_i^{n+1} - U_i^*}{\Delta t} = -\frac{1}{\rho}\frac{\partial (p^{n+1} - p^n)}{\partial x_i} \tag{7}$$

where p^n and p^{n+1} represent the pressure at the previous and current time step, respectively. U^* is intermediate velocities. Using the pressure projection again, we have:

$$\frac{\partial^2(p^{n+1}-p^n)}{\partial x_i \partial x_i} = \frac{\rho}{\Delta t}\frac{\partial U_i^*}{\partial x_i} \tag{8}$$

Like the NIPC scheme, the SIPC scheme first solves Eq. (6) with the implicit Euler scheme for the temporal term; semi-implicit scheme for convection term; and implicit scheme for the diffusion teem to obtain intermediate velocity U^*. Then the SIPC scheme solves the Poisson equation, Eq. (8), to obtain the pressure p^{n+1}. Finally, the SIPC scheme calculates the velocity at the next step U^{n+1} by solving Eq. (7) that is:

$$U_i^{n+1} = U_i^* - \frac{\Delta t}{\rho}\frac{\partial(p^{n+1}-p^n)}{\partial x_i} \tag{9}$$

Rotational incremental pressure-correction scheme

The NIPC scheme uses a non-physical Neumann boundary condition enforced on the pressure that is used on the numerical boundary layer. This consequently limits the accuracy of the scheme [22, 23], and will slightly modify Eq. (9) as:

$$U_i^{n+1} = U_i^* - \frac{\Delta t}{\rho}\frac{\partial \phi^{n+1}}{\partial x_i} \tag{10}$$

$$p^{n+1} = \phi^{n+1} + p^n - \nu\frac{\partial U_j^*}{\partial x_j} \tag{11}$$

The solving procedure is exactly the same with the SIPC scheme.

Non-incremental pressure-correction scheme with semi-Lagrangian scheme

The NIPC-SL scheme applies a three-step time-advancement scheme [24] that splits the momentum equation (Eq. (2)) into three discretized equations:

$$\frac{U_i^* - U_i^n}{\Delta t} = -U_j^n\frac{\partial U_i^n}{\partial x_j} \tag{12}$$

$$\frac{U_i^{**} - U_i^*}{\Delta t} = \nu\frac{\partial^2 U_i^{**}}{\partial x_j \partial x_j} + \frac{1}{\rho}F_i \tag{13}$$

$$\frac{U_i^{n+1} - U_i^{**}}{\Delta t} = -\frac{1}{\rho}\frac{\partial p}{\partial x_i} \tag{14}$$

where U^n and U^{n+1} represent the velocity at the previous and current time step, respectively. U^* and U^{**} are intermediate velocities. Using the pressure projection, we have:

$$\frac{\partial^2 p}{\partial x_i \partial x_i} = \frac{\rho}{\Delta t}\frac{\partial U_i^{**}}{\partial x_i} \tag{15}$$

The NIPC-SL scheme first solves Eq. (12) with the SL scheme to obtain intermediate velocity U^*. Then it solves the two Poisson equations, Eqs. (13) and (15), in sequence to obtain intermediate velocity U^{**} and pressure p, respectively. Finally, the algorithm calculates the velocity at the next step U^{n+1} by solving Eq. (14). In

OpenFOAM, the solution of Eqs. (13), (14), and (15) is straightforward. The semi-Lagrangian (SL) scheme applies the Lagrangian advection to a Euler grid so that it will remain stable at large time steps. The scheme traces the flow particle trajectory at each cell back in time to its former position, which is called the departure point, X_d, and copies the quantities at that position to the present cell, which is called the arrival point, X_a. The SL scheme actually solves Eq. (12) by:

$$U^*(X_a) = U^n(X_d) = U^n(X_a - \Delta t U^n(X_a)) \tag{16}$$

where $U^*(X_a)$ is the value of U^* at point X_a, and $U^n(X_d)$ is the value of U^n at point X_d. Since the departure point represents the position of the arrival point in the previous time step, $X_d = X_a - \Delta t U^n(X_a)$. To obtain $U^n(X_d)$, the SL scheme first identifies the index of the departure cell. Since the departure point X_d is not necessarily located at the cell center, $U^n(X_d)$ is estimated by interpolation from the values in the surrounding cells, and the result is set as $U^*(X_a)$ in Eq. (16).

D.2. Validation of fast fluid dynamics solvers

This study validated the accuracy and applicability of the developed FFD solvers when implemented in OpenFOAM for four indoor airflow cases. The first three cases were used to test the FFD models in predicting the steady-state indoor airflow. Experimental data was available for evaluating the accuracy of the FFD simulations. The last case was to test the FFD models in predicting transient indoor airflow. The CFD simulation with the SIMPLE algorithm was used as a reference.

Forced convection in a simplified room

This study tested the FFD solvers by the forced convection flow in a room from Wang and Chen [25]. Figure 1 (on the next page) shows a 2.44 m × 2.44 m × 2.44 m room with a plane jet from the upper left corner that developed along the ceiling and reached the far right. The inlet height was 0.03 m. The inlet air velocity was 0.455 m/s with a corresponding Reynolds number of around 2,000. The flow then moved downwards because of the existence of the right-side wall, and formed a circulation pattern in the room. The outlet height was 0.08 m. A box in the middle of the room, with dimensions of 1.22 m × 1.22 m × 1.22 m, was used to represent an object such as furniture. The temperatures of the box surface, ceiling, surrounding walls, floor, and supply air were identical. Therefore, the type of airflow in the room was forced convection.

This investigation applied the zero equation (0-eqn) model [26] to simulate the turbulence, since Wang and Chen [25] concluded that this model performs well for predicting the forced convection flow in an indoor environment. The turbulent viscosity is determined by the local mean air velocity $|\mathbf{U}|$ and a length scale that is the shortest distance L to the wall:

$$\nu_t = 0.03874 \,|\, \mathbf{U} \,|\, L \tag{17}$$

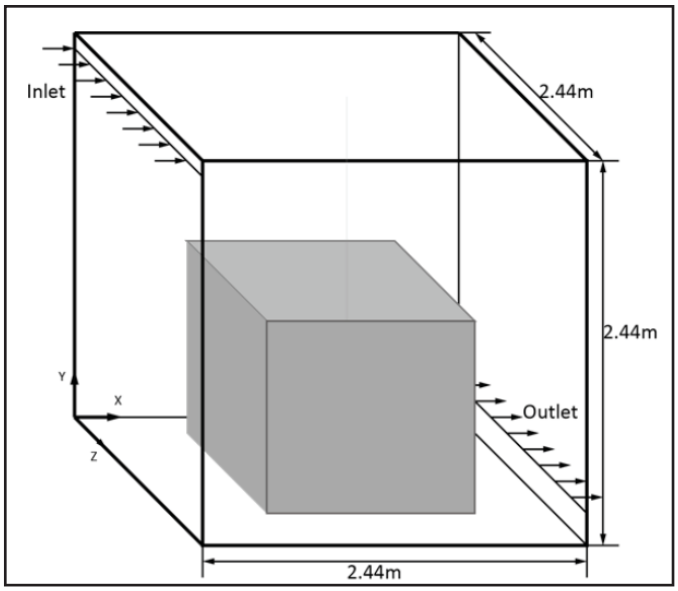

Figure 1: Sketch of the room with a box.

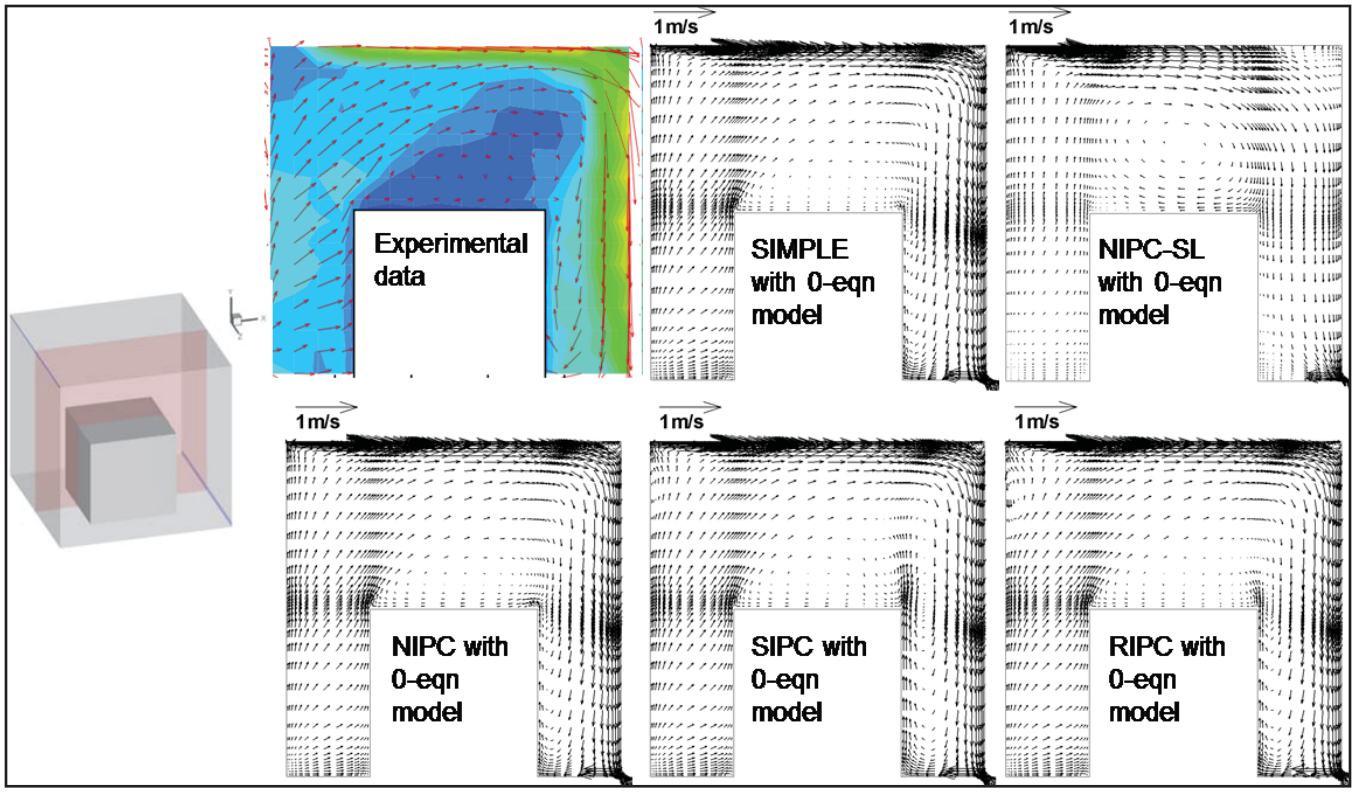

Figure 2: Airflow patterns (arrows) measured by Wang and Chen [25] and predicted by CFD and FFD with the 0-eqn model.

This study compared the simulated and measured velocity distributions in Figure 2 to assess the performance of FFD solvers. The CFD simulation used the SIMPLE algorithm and the 0-eqn model was also provided as a reference. In general, the velocity distributions, except the one predicted by NIPC-SL, were very similar to the measured ones. This is because the SL scheme added significant extra numerical diffusion.

However, it is difficult to make quantitative comparison in Figure 2. This study thus compared the calculated air velocity profiles with the measured data at four representative positions in the room, as shown in Figure 3 (on the next page). These positions are at the jet upstream, jet downstream, center of the room, and a location close to the side wall. The air velocity was normalized by U_{max} = 1.5 m/s. The CFD simulation used the SIMPLE algorithm and the 0-eq model to provide a fairly good prediction on the air velocity. The NIPC, SIPC, and RIPC with 0-eqn model had very similar performance, and the predicted air velocity profiles agree well with the experimental data. At position 1, we can notice an obvious difference between the predicted and measured air velocity, since the air velocity there was very small. With the added numerical diffusion, the NIPC-SL with 0-eqn model had the worst performance, as it under predicted the jet flow and re-circulated flow.

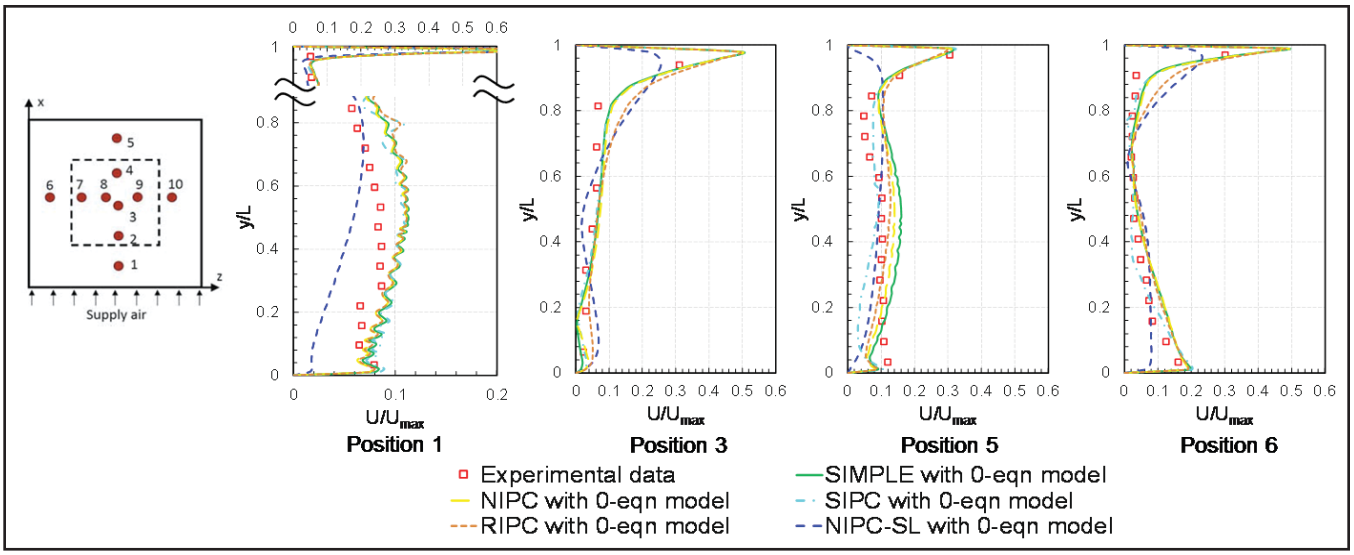

Figure 3: Comparison of air velocity profiles predicted by CFD and FFD with the 0-eqn model and the experimental data from Wang and Chen [25] at position 1, position 3, position 5, and position 6.

Mixed convection in a simplified room

Based on the case setup in Figure 1, this case added 700 W of heat inside of the box. All other experimental conditions were exactly the same as those for the abovementioned case. The supply air temperature was controlled at 22.2°C. The temperatures of the box surface, ceiling, surrounding walls, and floor were 36.7, 25.8, 27.4, and 26.9°C, respectively. The heated box could form a thermal plume. Therefore, the type of airflow in the room was mixed convection.

This investigation again applied the 0-eqn model to simulate the turbulence, since Zhang et al. [27] concluded that this model performs well for predicting the mixed convection flow in an indoor environment.

This study compared the simulated and measured velocity distributions in Figure 4 (on the next page). Again, the velocity distributions, except the one predicted by NIPC-SL, were very similar to the measured ones in general. This is because the SL scheme added significant extra numerical diffusion. To make quantitative comparison, this study compared the calculated air velocity profiles with the measured data at four representative positions in the room, as shown in Figure 5 (on the next page). The NIPC-SL with the 0-eqn model still performs poorly, as it under predicted the jet flow and re-circulated flow. The other schemes had similar performance and the predicted air velocity profiles with the 0-eqn model agreed well with the experimental data. This confirms the performance of FFD solvers. However, there is still significant difference at the lower part of position 5. This is because the flow there was very complicated, since the box and the jet interacted and generated a secondary recirculation. Wang and Chen [25] had tried more sophisticated models such as the Large Eddy Simulation, but it could not predict the measured velocity profile at this location either.

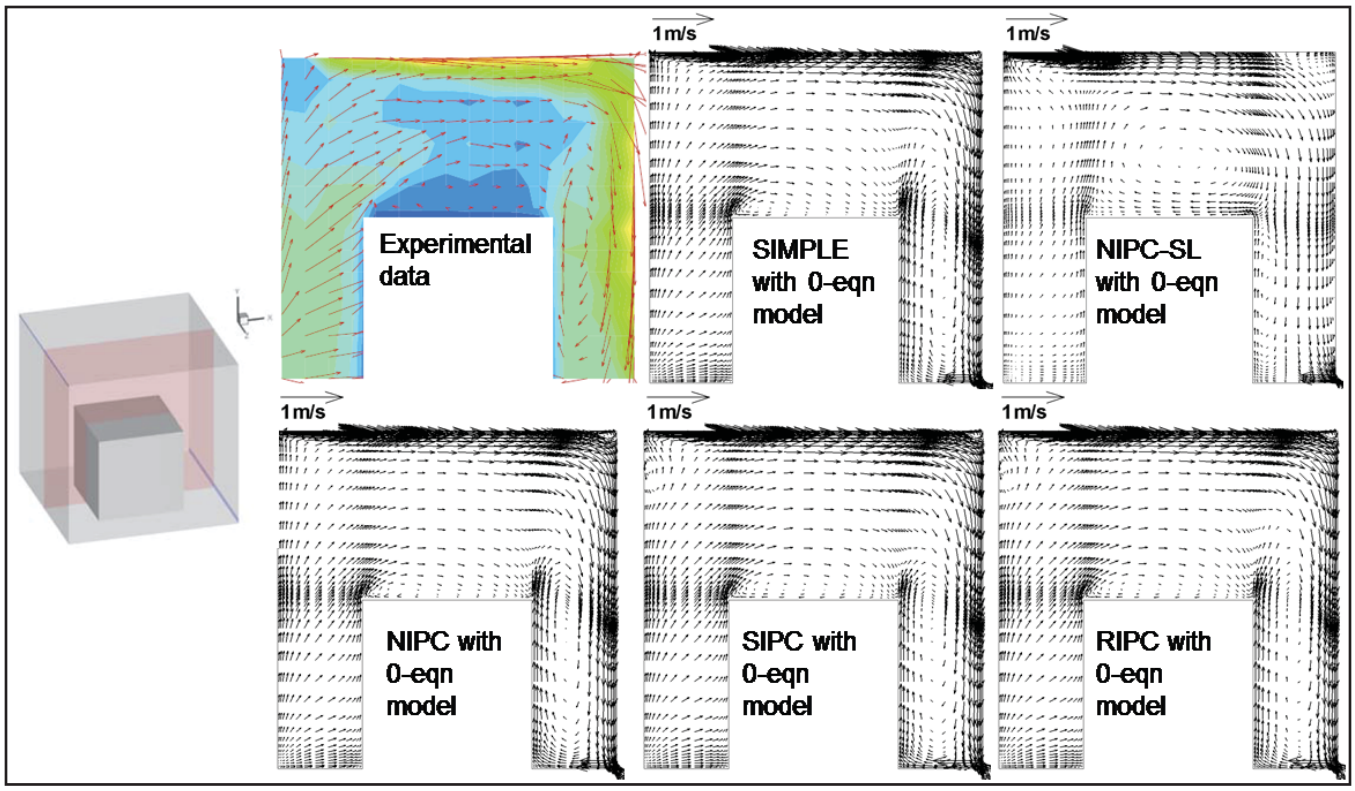

Figure 4: Airflow patterns (arrows) measured by Wang and Chen [25] and predicted by CFD and FFD with the 0-eqn model.

This case was non-isothermal and Figure 6 (on the next page) compares the predicted temperature profiles with the experimental data in the same positions as shown in Figure 5. The temperature was normalized by using T_{min} = 22.2°C and T_{max} = 36.7°C, which were the minimum and maximum temperatures, respectively, that were observed in this case. All the numerical simulations of air temperature agreed well with the experimental data.

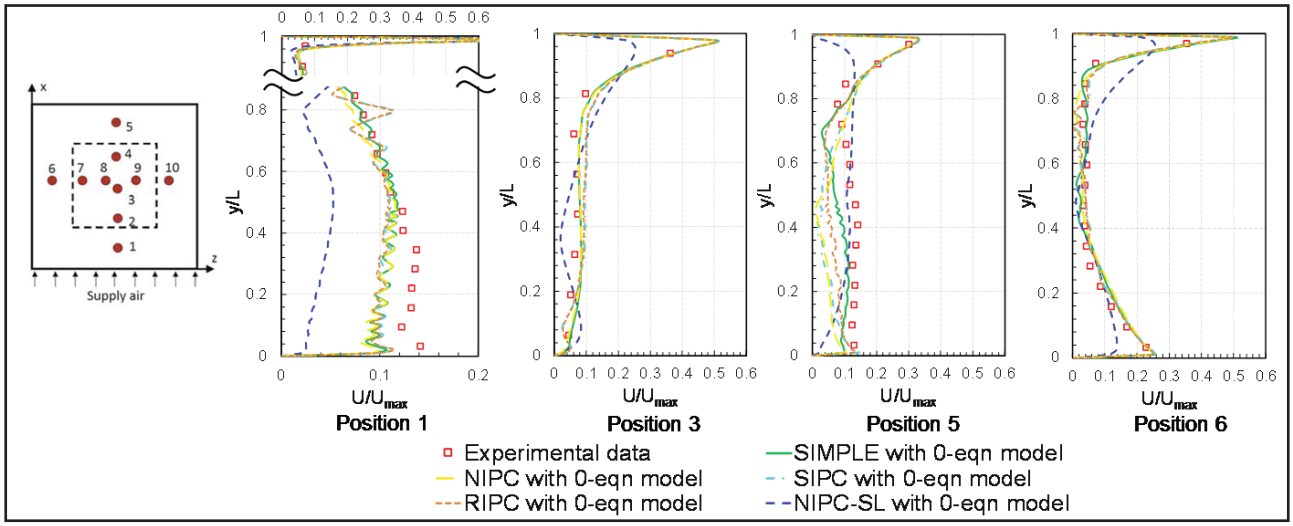

Figure 5: Comparison of air velocity profiles predicted by CFD and FFD with the 0-eqn model and the experimental data from Wang and Chen [25] at position 1, position 3, position 5, and position 6.

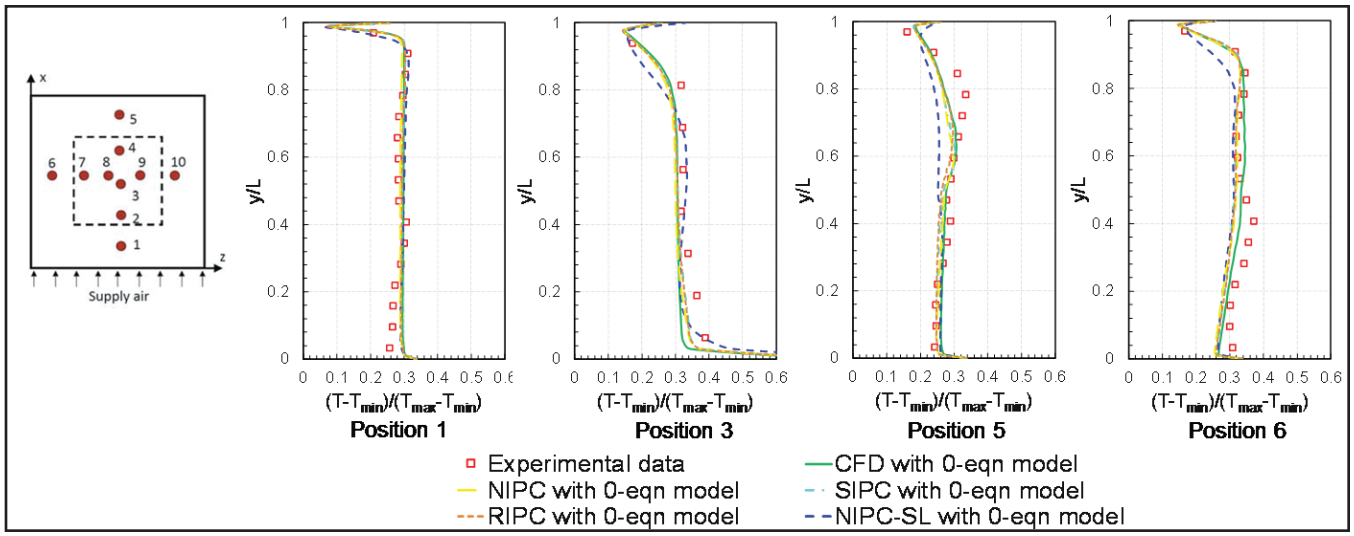

Figure 6: Comparison of air temperature profiles predicted by CFD and FFD with the 0-eqn model and the experimental data from Wang and Chen [25] at position 1, position 3, position 5, and position 6.

Displacement ventilation in an office

Figure 7 shows an occupied office with displacement ventilation [28]. The office was simulated by an experimental chamber of 5.16 m × 3.65 m × 2.43 m with a displacement diffuser on the side wall supplying air at a ventilation rate of 4 air changes per hour. The supply air temperature was 17°C. There are two occupants, two computers, two tables, two boxes, and six lamps in the room as shown in Figure 7(a). For detailed sizes, locations, and heat release of these items and other thermos-fluid boundary conditions, one can refer to Yuan et al. [28]. The experiment measured the air temperature and air velocity along nine vertical poles distributed in the stream-wise center plane and the cross-sectional center plane as shown in Figure 7(b). Figure 7(b) also shows the mesh used based on our grid independence test.

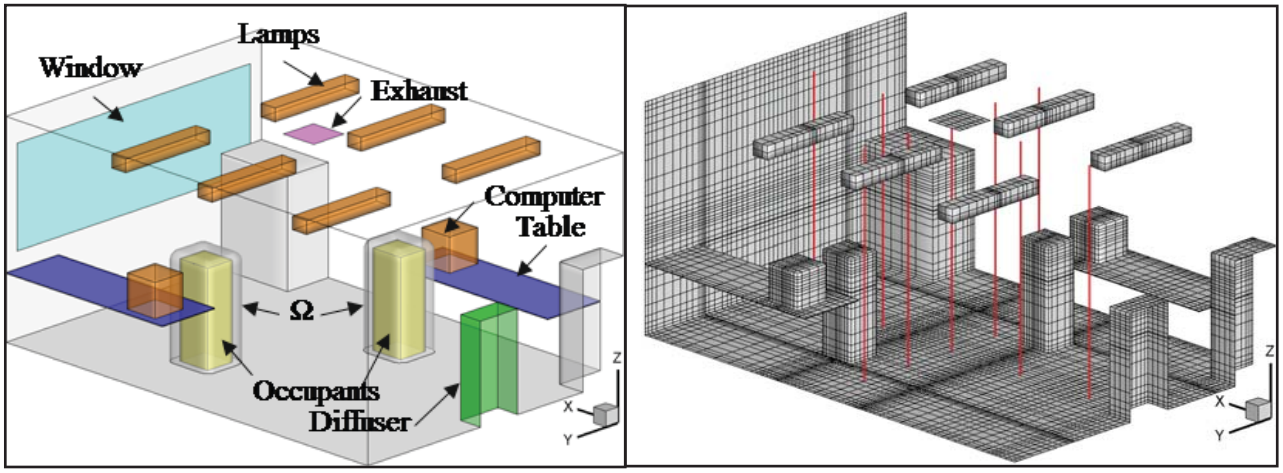

Figure 7: (a) Schematic and (b) mesh of displacement ventilation on an occupied office. The red vertical poles represent measurement locations for air velocity and temperature.

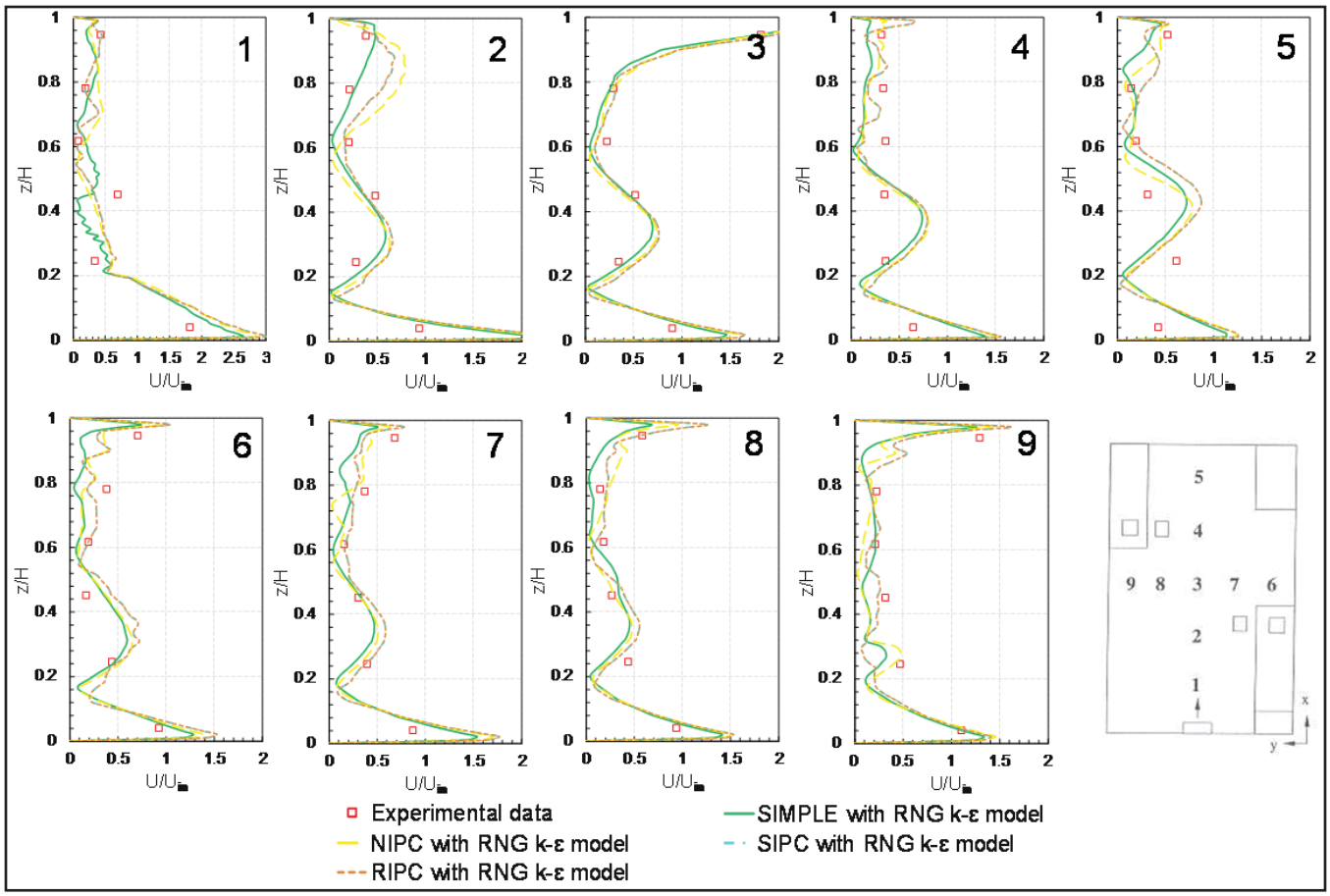

Figure 8: Comparison of air velocity profiles predicted by CFD and FFD with the RNG k-ε model and the experimental data from Yuan et al. [28]

Since this is a much more close-to-real case, this study applied the RNG k-ε model to simulate the turbulence. Due to the poor performance of NIPC-SL in the previous two cases, this study did not consider this numerical scheme for this case. The CFD simulation used SIMPLE algorithm was again provided as a reference.

This study compared the calculated air velocity profiles with the measured data at the nine positions in the room, as shown in Figure 8. The air velocity was normalized by the inlet air velocity U_{in} = 0.09 m/s. The quantitative agreement between the predicted and measured air velocity is good. All the projection methods had almost the same performance and it is hard to determine if the SIMPLE algorithm or projection methods have better performance. Figure 9 further compared the calculated air temperature profiles with the measured data at the nine positions in the room. The normalized air temperature θ was defined as $(T - T_s)/(T_r - T_s)$, where T_s (supply air temperature) = 17.0°C and T_r (return air temperature) = 26.7°C. Again, the quantitative agreement between the predicted and measured air temperature is good. It implies that the projection methods without SL scheme has no worse performance than the SIMPLE algorithm in predicting steady-state flow in indoor environment.

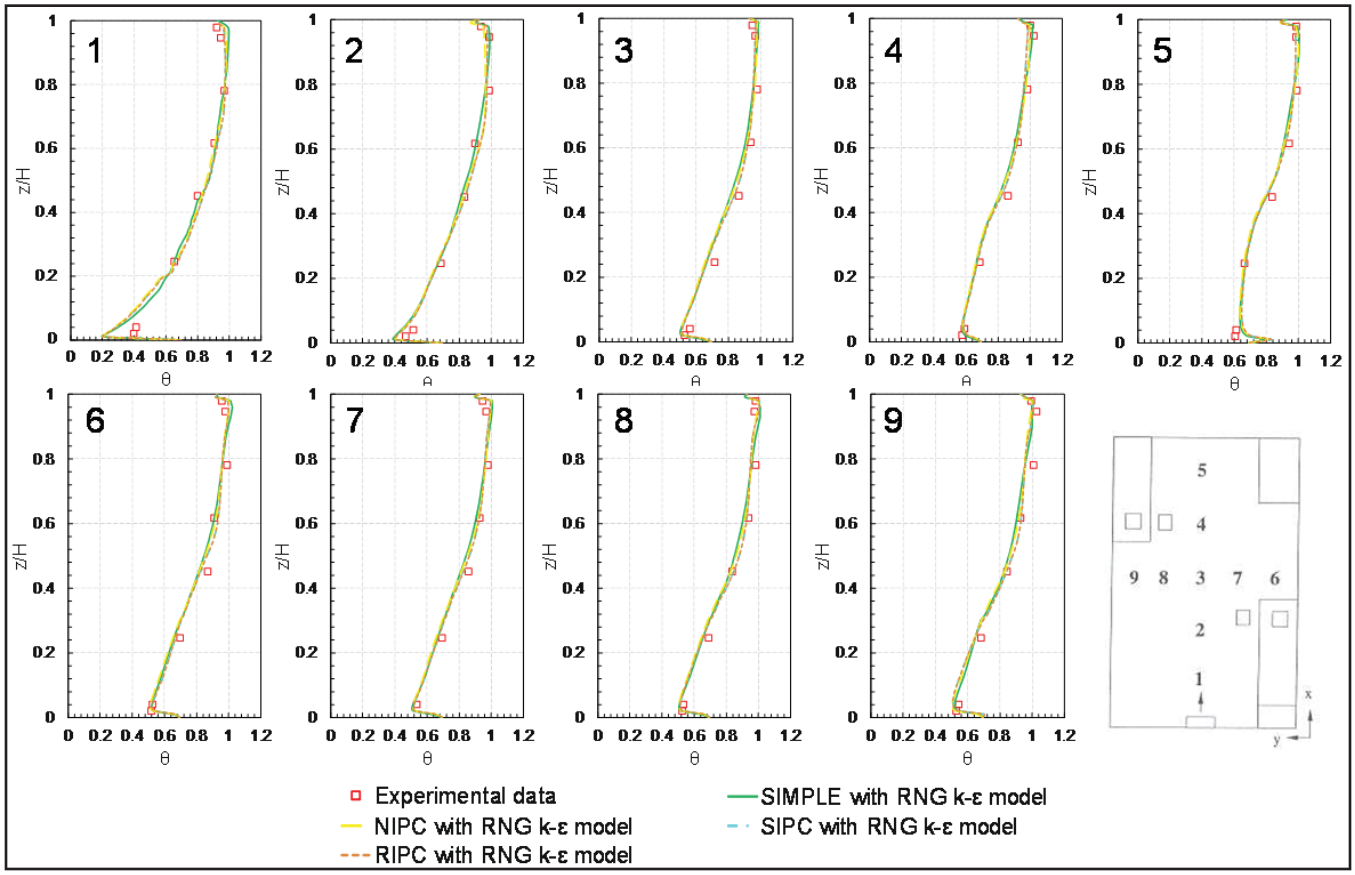

Figure 9: Comparison of air temperature profiles predicted by CFD and FFD with the RNG k-ε model and the experimental data from Yuan et al [28].

Mixed convection in a 2D cavity

The last case this study used was to validate the performance of projection methods in predicting transient flow in an indoor environment. It was a two-dimensional, non-isothermal case with experimental data [29]. In Figure 10 (on the next page), the dimensions of the flow domain were H × H = 1.04 m × 1.04 m; the inlet height was h_{in} = 18 mm; and the outlet height was h_{out} = 24 mm. In the experiment, the inlet air velocity was U_x = 0.57 m/s, U_y = 0.0 m/s, and the inlet air temperature (T_{in}) was 15°C. The temperature of the walls (T_{wl}) was 15°C, and that of the floor (T_{fl}) was 35.5°C to form a thermal plume. The case used here is representative of airflows in enclosed environments as it includes major flow characteristics in an indoor environment, such as jets and thermal plumes. Furthermore, it was not desirable to use very complex cases for this investigation since those cases may have uncertainties. Instead, this simple two-dimensional case, but still with complex flow features, was more desirable for validation. Since the experiment did not measure the transient flow fields, this study used the predicted airflow by CFD simulation with the SIMPLE algorithm as a reference. To eliminate the possible error brought by turbulence models, this study adopted the RNG k-ε model that is much more sophisticated than the 0-eqn model to simulate the turbulence.

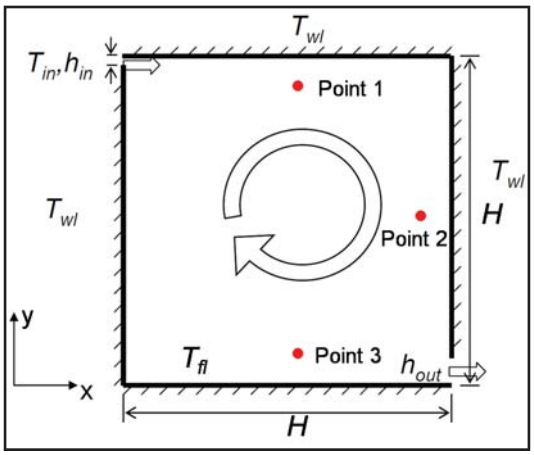

Figure 10: Sketch of the two-dimensional, non-isothermal case.

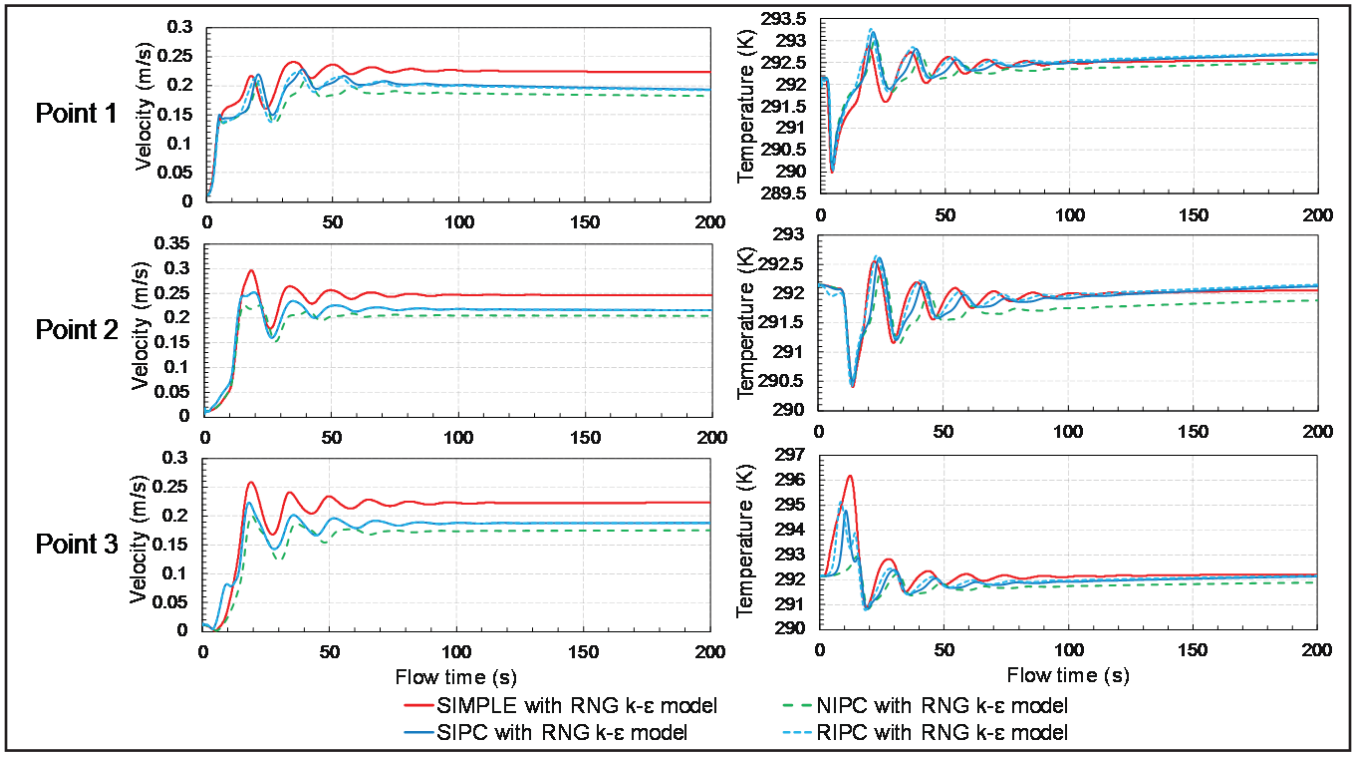

Figure 11: Monitored transient air velocity and temperature at points 1, 2, and 3 (refer to Fig. 10).

This study monitored the transient air velocity and temperature at three typical locations—points 1, 2, and 3 (refer to Fig. 10) as shown in Figure 11. These locations were selected because they were at the jet downstream, the outlet, and the flow recirculation area. The predicted transient air velocity determined by the projection methods has the same features as predicted by the SIMPLE algorithm. We can also notice the difference in velocity magnitude, however, the difference was as small as 0.025 m/s. For the monitored air temperature, the predictions by the NIPC scheme have minor differences from the predictions of the other algorithms or schemes. Overall, the SIPC and RIPC performed very similarly and their predictions had better agreement with those predicted by the SIMPLE algorithm.

Figure 12 (on the next page) further compared the predicted flow fields at t = 5 s, 10 s, 15 s, and 25 s, when the flow fields changed significantly. It is clear that all the projection methods could capture the flow features

as the SIMPLE algorithm did. For all the algorithms or schemes, this study calculated the flow for physical time of 200 s with a time step size of 0.05 s. The selected time step size could ensure the Courant number to be less than 1. Both FFD and CFD simulations were performed with the same structured mesh on a personal computer with a single CPU core at 3.50 GHz. The computing time for FFD simulations was 0.6 mins and that for CFD simulations was 23.6 mins. FFD was almost 40 times faster than CFD in predicting the transient flow and the similar prediction accuracy could be maintained.

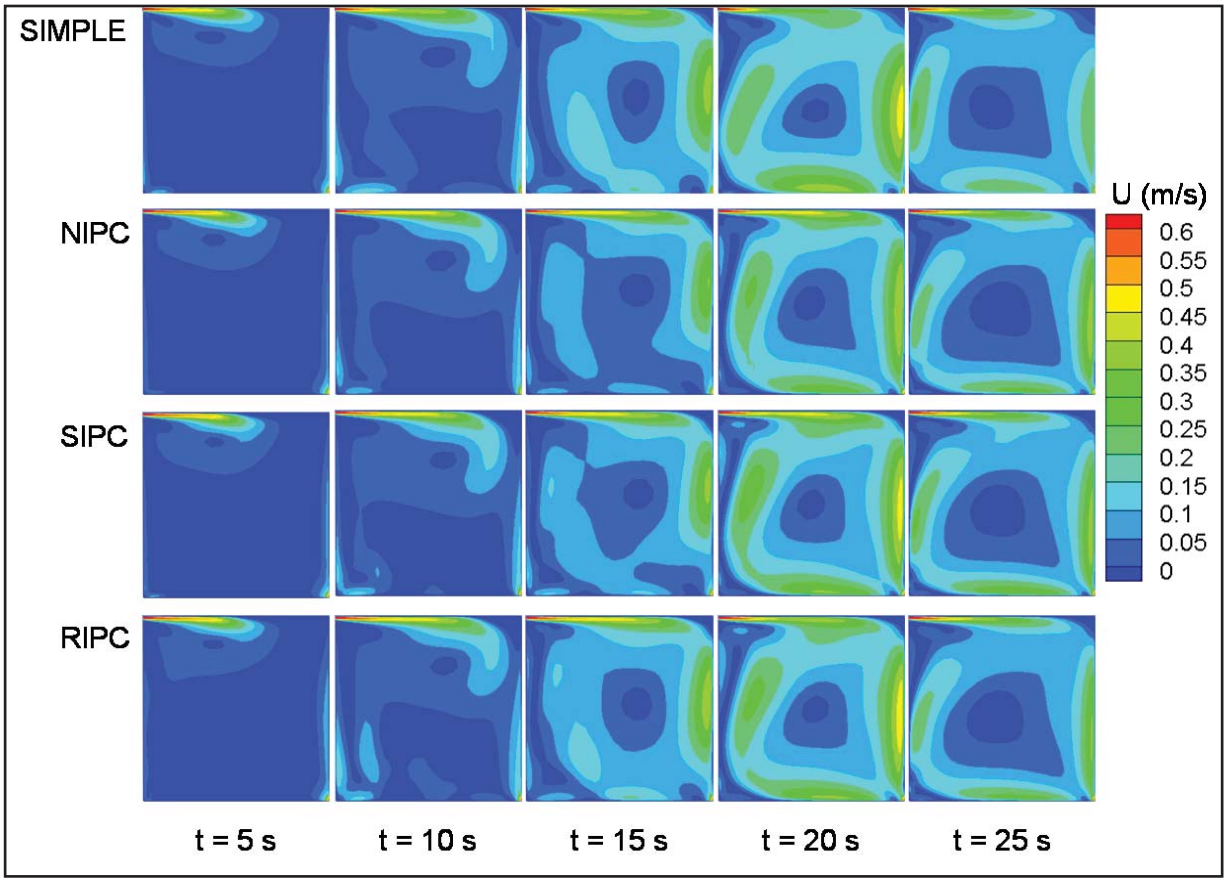

Figure 12: Predicted flow fields at t = 5 s, 10 s, 15 s, and 25 s, respectively.

E. Milestones

- June 30, 2016: Development and validation for FFD solvers
- June 30, 2017: Development of user interface for FFD solvers

F. Future Plans

Although most engineers are familiar with computer assisted tools from other areas of work, FFD simulations typically represent a level of computational complexity that is significantly beyond their existing skill set and cannot be quickly acquired. To remedy the problem, we plan to further develop a graphical interface previously developed by the principal investigator, SCI, as shown in Figure 13 (on the next page). SCI is a public domain program designed to alleviate the stresses placed on non-expert users in running FFD with the program developed in this report as its engine. SCI allows air distribution designers to create, run, and view a simulation using user interface paradigms that they are familiar with. In the creation phase, SCI will be developed to convert CAD files into the mesh cells required for the FFD engine. The user can provide a shell

description of the problem to be simulated, including air velocity, temperature, species concentrations, etc., as well as the desired computational accuracy. The interface shown in Figure 13 will remain more or less the same, as it has been field tested by building designers. These parameters are well understood, and it is not difficult for designers to provide useful values, or understand their effects on the results. Intelligent groupings, default values, and parameter elimination will be used continuously to reduce and combine many of the parameters that may not be familiar to designers. After the model has been created, SCI will be able to run the FFD solver. Finally, the results will be immediately visualized in SCI as shown in Figure 13(c).

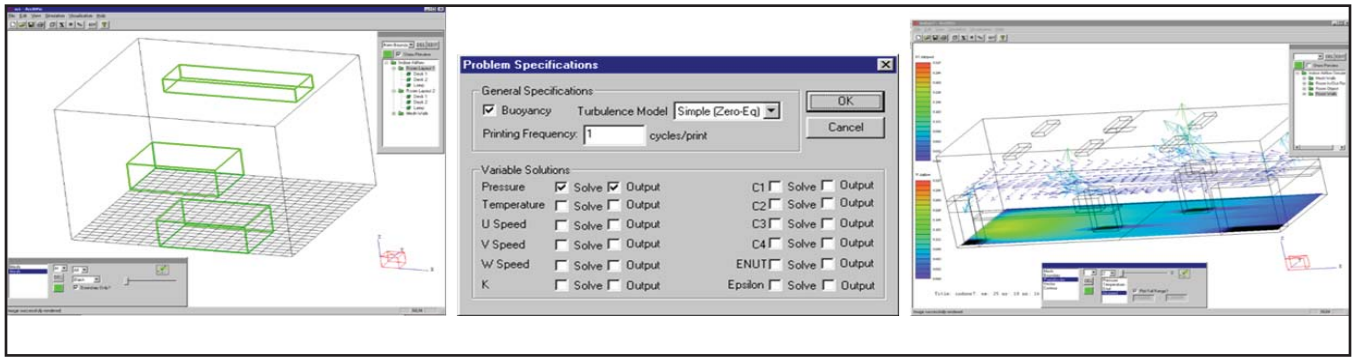

(a) (b) (c)

Figure 13: SCI interface: (a) geometry and meshes, (b) computational parameter specification, and (c) result visualization.

III. RELEVANCE AND TRANSITION

A. Relevance of Research to the DHS Enterprise

Terrorists have used explosives in the past against civilians. Airports and water ports are attractive targets for terrorists—especially shipping containers, of which, only 2% are physically examined. The risk is too high for us to accept. Our research will produce a method that can quickly predict explosives transport in water ports and airports. This will make the United States safer.

B. Potential for Transition

- The numerical tools developed by this project can be used at water ports and airports in the United States and abroad for predicting explosives transport.
- This project will provide crucial information for explosives vapor sensor developers.

C. Data and/or IP Acquisition Strategy

The explosives detection systems are to be developed with IP and will be transferred to relevant authorities with a suitable agreement to be established by the ALERT Center of Excellence.

D. Transition Pathway

We will work closely with the sensor developers in Thrust 2 so that we can have a better understanding of the sensor performance. We can use the sensor sensitivity to design the explosives detection systems.

E. User or Customer Connections

Bill Reardon
TSA Chief
Indianapolis International Airport
317-487-5385
breardon@indianapolisairport.com

Michael Medvescek, A.A.E., A.C.E.
Sr. Director of Operations
Indianapolis Airport Authority
7800 Col. H. Weir Cook Memorial Dr.
Indianapolis, IN 46241
317-487-5024
mmedvescek@ind.com

IV. PROJECT ACCOMPLISHMENTS AND DOCUMENTATION

A. Education and Workforce Development Activities

1. Course, Seminar, and/or Workshop Development

   We intend to revise ME522 "Indoor Environment Analysis and Design" at Purdue University by using the research results obtained from this project.

B. Peer Reviewed Journal Articles

1. Wei Liu, Mingang Jin, Chun Chen, Ruoyu You, Qingyan Chen. "Implementation of a fast fluid dynamics model in OpenFOAM for simulating indoor airflow." *Numerical Heat Transfer, Part A: Applications*. January 2016, 69(7), pp. 748-762.

C. Software Developed

1. Models
   a. Fast Fluid Dynamics program implemented to OpenFOAM computer program.

V. REFERENCES

[1] Q. Chen, Ventilation performance prediction for buildings: A method overview and recent applications, Building and Environment, vol. 44, no. 4, pp.848-858, 2009.
[2] Q. Chen, K. Lee, S. Mazumdar, S. Poussou, L. Wang, M. Wang, and Z. Zhang, Ventilation performance prediction for buildings: Model assessment, Building and Environment, vol. 45, no. 2, pp.295-303, 2010.
[3] L. Wang and Q. Chen, Evaluation of some assumptions used in multizone airflow network models, Building and Environment, vol. 43, no. 10, pp.1671-1677, 2008.
[4] A. C. Megri and F. Haghighat, Zonal modeling for simulating indoor environment of buildings: Review, recent developments, and applications, HVAC&R Research, vol. 13, no. 6, pp.887-905, 2007.
[5] C. H. Lin, R. H. Horstman, M. F. Ahlers, L. M. Sedgwick, K. H. Dunn, J. L. Topmiller, J. S. Ben-nett, and S. Wirogo, Numerical simulation of airflow and airborne pathogen transport in aircraft cabins–

Part I: Numerical simulation of the flow field, ASHRAE Transactions, vol. 111, no. 1, pp.755-763, 2005.

[6] T. N. Krishnamurti, Numerical integration of primitive equations by a quasi-Lagrangian advective scheme, Journal of Applied Meteorology, vol. 1, no. 4, pp.508-521, 1962.

[7] A. Robert, A stable numerical integration scheme for the primitive meteorological equations, Atmosphere-Ocean, vol. 19, no. 1, pp.35-46, 1981.

[8] A. Staniforth and J. Côté, Semi-Lagrangian integration schemes for atmospheric models–A review, Monthly Weather Review, vol. 119, no. 9, pp 2206-2223, 1991.

[9] D. Caya and R. Laprise, A semi-implicit semi-Lagrangian regional climate model: The Canadian RCM, Monthly Weather Review, vol. 127, no. 3, pp.341-362, 1999.

[10] J. Stam, Stable fluids, Proceedings of the 26th annual conference on computer graphics and interactive techniques, ACM Press/Addison-Wesley Publishing Co, 1999.

[11] W. Zuo and Q. Chen, Real time or faster-than-real-time simulation of airflow in buildings, Indoor Air, vol. 19, no. 1, pp.33-44, 2009.

[12] W. Zuo, J. Hu, and Q. Chen, Improvements on FFD modeling by using different numerical schemes, Numerical Heat Transfer, Part B: Fundamentals, vol. 58, no. 1, pp.1-16, 2010.

[13] W. Zuo, M. Jin, and Q. Chen, Reduction of numerical diffusion in the FFD model, Engineering Applications of Computational Fluid Mechanics, vol. 6, no. 2, pp.234-247, 2012.

[14] M. Jin, W. Zuo, and Q. Chen, Improvements of fast fluid dynamics for simulating airflow in buildings, Numerical Heat Transfer, Part B: Fundamentals, vol. 62, no. 6, pp.419-438, 2012.

[15] M. Jin, W. Zuo, and Q. Chen, Simulating natural ventilation in and around buildings by fast fluid dynamics, Numerical Heat Transfer, Part A: Applications, vol. 64, no. 4, pp.273-289, 2013.

[16] M. Jin and Q. Chen, Improvement of fast fluid dynamics with a conservative semi-Lagrangian scheme, International Journal of Numerical Methods for Heat and Fluid Flow, vol. 25, no. 1, pp.2-18, 2015.

[17] OpenFOAM, The Open Source CFD Toolbox, http://www.opencfd.co.uk/openfoam.html, 2007.

[18] A. J. Chorin, Numerical solution of the Navier–Stokes equations, Math. Comput. 22, pp.745–762, 1968.

[19] R. Temam, Sur l'approximation de la solution des e´quations de Navier–Stokes par la me´thode des pas fractionnaires ii, Arch. Ration. Mech. Anal. 33, pp.377–385, 1969.

[20] A. J. Chorin, A numerical method for solving incompressible viscous flow problems, Journal of Computational Physics, vol. 2, no. 1, pp.12-26, 1967.

[21] K. Goda, A multistep technique with implicit difference schemes for calculating two- or three-dimensional cavity flows, J. Comput. Phys. 30, pp.76–95, 1979.

[22] J.-L. Guermond, P. Minev, J. Shen, Error analysis of pressure-correction schemes for the Navier–Stokes equations with open boundary conditions, SIAM J. Numer. Anal. 43 (1), pp.239–258, 2005.

[23] L.J.P. Timmermans, P.D. Minev, F.N. Van De Vosse. An approximate projection scheme for incompressible flow using spectral elements, Int. J. Numer. Methods Fluids 22, pp.673–688, 1996.

[24] J. H. Ferziger and M. Perić, *Computational Methods for Fluid Dynamics*, Berlin: Springer, vol. 3, pp.196-200, 2002.

[25] M. Wang and Q. Chen, Assessment of various turbulence models for transitional flows in enclosed environment, HVAC&R Research, vol. 15, no. 6, pp.1099-1119, 2009.

[26] Q. Chen and W. Xu, A zero-equation turbulence model for indoor airflow simulation. Energy and buildings, 28(2), pp.137-144, 1998.

[27] Z. Zhang, W. Zhang, Z. Zhai, and Q. Chen, Evaluation of various turbulence models in predicting airflow and turbulence in enclosed environments by CFD: part-2: comparison with experimental data from literature, HVAC&R Research, 13(6), pp.871-886, 2007.

[28] X. Yuan, Q. Chen, L. R. Glicksman, Y. Hu, and X. Yang, Measurements and computations of room airflow with displacement ventilation. Ashrae Transactions, 105, p.340, 1999.

[29] D. Blay, S. Mergui, and C. Niculae. Confined turbulent mixed convection in the presence of a horizontal

buoyant wall jet. Fundamentals of Mixed Convection, 213, pp.65–72, 1992.

This page intentionally left blank.